Thermal and mechanical response of particulate composite plates under inertial excitation

Jacob K. Miller, Daniel C. Woods, and Jeffrey F. Rhoads
School of Mechanical Engineering, Ray W. Herrick Laboratories and Birck Nanotechnology Center, Purdue University, West Lafayette, Indiana 47907, USA

(Received 16 September 2014; accepted 5 December 2014; published online 24 December 2014)

The thermal and mechanical, near-resonant responses of particulate composite plates formed from hydroxyl-terminated polybutadiene (HTPB) binder and varying volume ratios of ammonium chloride (NH_4Cl) particles (50, 65, 75%) are investigated. Each test specimen is clamped and forced with three levels of band-limited, white noise inertial excitation (10–1000 Hz at 1.00, 1.86 and 2.44 g RMS). The mechanical response of each plate is recorded via scanning laser Doppler vibrometry. The plates are then excited at a single resonant frequency and the thermal response is recorded via infrared thermography. Comparisons are made between the mechanical operational deflection shapes of each plate and spatial temperature distributions, with correlation seen between the observed level of strain, as visualized by strain energy density, and heat generation. The effect of particle/binder ratio on both the thermal and mechanical responses is discussed. Acquired results are also compared to an analytical model of the system. The observed thermomechanical effects render an improved understanding of the thermomechanics of plastic-bonded composites, an essential step in support of the development of new technologies for the vapor-based detection of hidden explosives. © *2014 AIP Publishing LLC*. [http://dx.doi.org/10.1063/1.4904439]

I. INTRODUCTION

The detection of hidden explosive threats is essential for both national security and defense. While a wide array of detection systems are currently in development or use, the most popular seek to leverage trace vapor detection.[1,2] Despite the potential of this approach, the trace vapor detection of composite explosives remains a significant technical challenge due to their comparatively low vapor pressures.[2,3]

Interestingly, the vapor pressures of many explosive materials are greatly affected by temperature[1,3] and may be significantly increased with even slight (5 °C) rises in temperature. An increase in vapor pressure leads to a higher concentration of target vapors in the surrounding medium, which in turn facilitates easier detection.[3] Accordingly, the induction of heat within such materials may prove effective in increasing the detection probabilities associated with a variety of stand-off detection technologies.

In many pure materials and alternative composites, heat generation in response to acoustic and ultrasonic excitation is a well-studied effect. Prior investigations have highlighted, for example, the fact that heating within materials due to cyclic deformation is often attributable to a phase delay between fluctuating stress and strain fields.[4] Likewise, in the context of vibrothermography, Renshaw[5] and others [6–8] have shown that high-frequency excitation is highly effective at eliciting thermal responses near stress concentrations, such as cracks, voids, and inclusions. While most of the prior work in thermography specifically targets heating near defects, research in this area has also highlighted stress-induced heating along the modal structure of various systems.[9–11] As vibrothermography is primarily used in the nondestructive testing of damaged samples, excitation at structural resonance is generally avoided, as heating from modal deflection patterns masks that which is associated with structural damage effects.[12] In the context of the present work, it is expected that modal heating will be more broadly applicable than defect-scale heating. As low-frequency excitations are amenable to the excitation of low-order modes, the thermal response of particulate composite materials, particularly plastic-bonded explosives, to such low-frequency acoustic or mechanical excitations is of distinct interest. Of course, an additional benefit of low-frequency excitation is its relatively large air propagation distance as compared with higher-frequency waves.

While mechanically induced heat generation is a well-studied effect in general, few thorough studies of the thermomechanics of particulate composite materials, such as plastic-bonded explosives, to low-frequency excitations currently exist. While the works of Loginov[13,14] provide some insight in this regard, these works focus largely on the phenomenological nature of the heating, rather than its selective control or the impact of the material's particle/binder ratio. Prior works have documented how the material properties of particulate composites vary with the aforementioned particle/binder ratio. Not surprisingly, these works have revealed that the bulk thermal and mechanical modulii of such materials vary dramatically with particle/binder ratio.[15–18] For example, Lewis[18] observed an inverse relationship between particle/binder ratios and damping ratios and noted that this relationship may be attributable to mismatched thermal expansion coefficients.

The objectives of this work are to observe and characterize the thermal and mechanical responses of particulate composite plates comprised of hydroxyl-terminated polybutadiene (HTPB) binder and ammonium chloride (NH_4Cl) particles under low-frequency (10–1000 Hz) inertial

 © 2014 AIP Publishing LLC

[This article is copyrighted as indicated in the article. Reuse of AIP content is subject to the terms at: http://scitation.aip.org/termsconditions. Downloaded to] IP: 128.211.168.1 On: Tue, 30 Dec 2014 20:52:05

excitation. This work serves as an extension to prior experiments detailing the thermomechanical response of HTPB-NH_4Cl beams[19] by highlighting the effects associated with changes in the ratio of crystal to binder. The plates themselves serve as mechanical mocks of common plastic-bonded energetic materials. For testing purposes, the plates were mounted directly to an electrodynamic shaker to deliver the greatest possible excitation forces. It should be noted that significant differences may be expected between direct shaker excitation and the previously mentioned acoustic excitation, and that the former excitation is employed in order to directly isolate the thermomechanics of the materials in question. Heat generation induced via this external excitation was quantified at various resonant frequencies through infrared thermography. The dependence of heat generation on the material's particle/binder ratio is discussed. As previously highlighted, the authors hope that the observed thermal effects will help render an improved understanding of the thermomechanics of plastic-bonded composites, an essential step in support of the development of new technologies for the vapor-based detection of hidden explosives.

II. EXPERIMENTAL TECHNIQUES

A. Sample preparation

As noted above, this work focuses on the thermomechanics of a mock plastic-bonded explosive material comprised of an HTPB binder and NH_4Cl particles. HTPB is a commonly employed binder material and the NH_4Cl particles were chosen in order to approximate the particle sizes of ammonium perchlorate (AP), an energetic material. The volume ratio of particle to binder may vary significantly in real-world explosives, and the effect of such changes on the mechanical and thermal responses of the bulk material is of importance in this paper.

To create the test samples, the HTPB was heated to 60 °C and an isocyanate hardening agent was applied. A wetting agent, Tepanol, was employed before the insertion and mixing of the NH_4Cl particles. For samples of high volume ratio, a Resodyn acoustic mixer was employed to ensure a homogeneous mixture. The particle/binder mixture was then poured into a purpose-built plate mold, and each was cured overnight into plates measuring 25.4×17.8 cm (10×7 in). For the purposes of this paper, three types of plates were used: 50, 65, and 75% volume ratio of particle to binder. The mass and density of all plates used in experimental testing are presented in Table I. It is important to note that these plates had different ages (recorded in terms of the number of days from mold release to testing) and that the mechanical response of this particular HTPB/NH_4Cl system has been observed to change over time.[20] As noted in the table, all of the 75% volume fraction plates are significantly less dense than the 50 and 65% volume fraction plates. Given that the density of the particle is significantly greater than that of the binder, this effect was not expected and is likely due to voids in the material. Difficulties in packing the more dense mixture into the mold were also noted.

TABLE I. Plate material properties.

Volume fraction-sample	Mass (kg)	Density (kg/m^3)	Approximate age (Days)
50%-1	0.6656	1154	450
50%-2	0.6593	1149	360
65%-1	0.8189	1297	450
65%-2	0.7162	1196	360
75%-1	0.6460	1086	450
75%-2	0.6354	1118	280
75%-3	0.5940	1031	280

B. Experimental setup

To provide mechanical excitation to the plates, a TIRA 59335/LS AIT-440 electrodynamic shaker was employed, which allowed for band-limited white noise inertial excitation. The system was controlled by a VibeLab VL-144 vibration control system through the direct monitoring of a shaker-head-mounted accelerometer. A custom plate fixture was machined to simulate clamped boundaries on the opposite short ends of the plates, approximating clamped-free-clamped-free (CFCF) boundary conditions. The final setup yielded a 22.9×17.8 cm (9×7 in.) unsupported area. To record the frequency responses and operational deflection shapes (ODS) of each plate, a Polytec PSV-400 scanning laser Doppler vibrometer was employed.

For the purposes of mechanical analysis, broadband (10–1000 Hz) white noise was applied at three distinct forcing levels (1.0, 1.9, and 2.4 g RMS). Operational deflection shapes were recorded at direct, 6 g forcing and were not seen to qualitatively change with excitation level. The system response was estimated through the application of the classical H1 estimator, a comparison of the measured cross-spectral density between the accelerometer and differentiated vibrometer readings to the measured power spectral density of the accelerometer. H1 frequency response estimators were calculated at all forcing levels at two distinct points; the geometric center of the plate and an "offset" point. The latter point was offset from the center by 6.2 and 4.8 cm as measured from the free and clamped edges, respectively. Geometrically, the offset traverses 54.6% and 54.2% of the distances between the center point and the free and clamped edges, respectively.

For the thermal analysis, the level of forcing was 2 g. It is important to note that the resonant frequency of each plate was seen to shift to lower frequencies by as many as 6 Hz over the 60 min trial. However, the frequency of excitation was set at the onset of testing and was not updated throughout the trials. To investigate the effect of this detuning, narrow-banded white noise excitation was applied to a 75% particle/binder ratio plate in a one-off experiment. The frequency extents of this band-limited white noise signal were chosen such that the plate was excited within the half-power bandwidth of the first resonant peak throughout the entire trial, and the total input acceleration was limited to 2 g RMS. The transient thermal behavior observed from this excitation was nearly identical to the direct excitation case. This suggests that, while the detuning effects remain unaccounted for, the thermal data recorded for direct sinusoidal excitation

[This article is copyrighted as indicated in the article. Reuse of AIP content is subject to the terms at: http://scitation.aip.org/termsconditions. Downloaded to] IP: 128.211.168.1 On: Tue, 30 Dec 2014 20:52:05

are still quite valid. All thermal data presented for the remainder of this paper were thus recorded with direct excitation at a stationary excitation frequency.

A FLIR A325 thermal camera was used to record both the transient and steady-state thermal responses of the surfaces of each plate. The thermal camera had a temperature sensitivity of 0.07 °C at 30 °C and accuracy of ±2 °C or ±2%. The infrared data were calibrated to the emissivity of each plate through a comparison to a thermocouple at ambient conditions. For this testing, the plates were excited at resonance for 60 min. The ambient temperature variation was also recorded, through the infrared observation of a small area of the testing rig, and was subtracted from the presented experimental data to negate a portion of the thermal noise and ambient temperature variations. This temperature was generally seen to rise approximately 0.5 °C throughout the 60 min trials, due to heating of the electrodynamic shaker. The influence of this rise cannot be exactly quantified but, as the ambient temperature is subtracted from the temperature data presented herein, it can only serve to partially mask the viscoelastic heating of the plates themselves. A picture of the entire experimental setup, in the thermal measurement configuration, is presented in Figure 1.

III. RESULTS

A. Mechanical response

The vibrometer-recorded H1 frequency response estimators for a representative plate in response to three levels of excitation are presented as Figures 2–4 for the 50, 65, and 75% plates, respectively. H1 estimators for the remaining plates of each volume fraction are not presented here for brevity but are qualitatively similar to those presented in the figure. These plots present data at both the center and offset points. Note that all of the plates exhibit clear resonant behavior, with multiple sharp peaks observable over the excited frequency range. The 65% and 75% plates show a slightly softening response, with peaks decreasing slightly in both amplitude and frequency as the forcing increases. Several plates within these sets also exhibit a split "first" mode, with the 75%–1 sample being the most severe. Qualitatively, the higher volume fraction plates appear to have more highly damped responses and much smoother response curves. The experimentally obtained peak frequencies for each plate (recorded from the highest excitation level utilized in the random vibration tests) are presented in Table II. Each observed mode is titled by a two-number descriptor which represents the increasing mode order in the

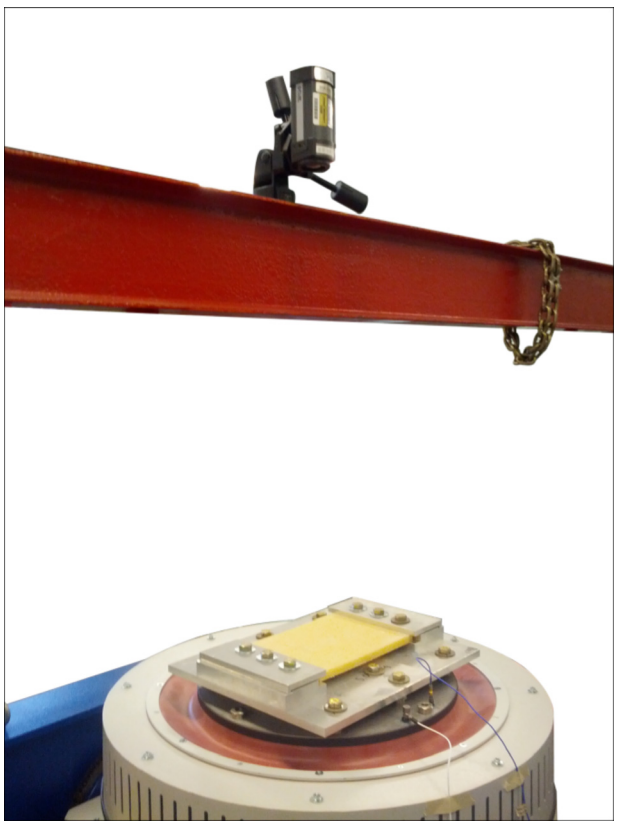

FIG. 1. The experimental setup. Here, a FLIR A325 infrared camera is positioned above a 50% particle/binder ratio plate mounted to the TIRA shaker by the CFCF clamping mount.

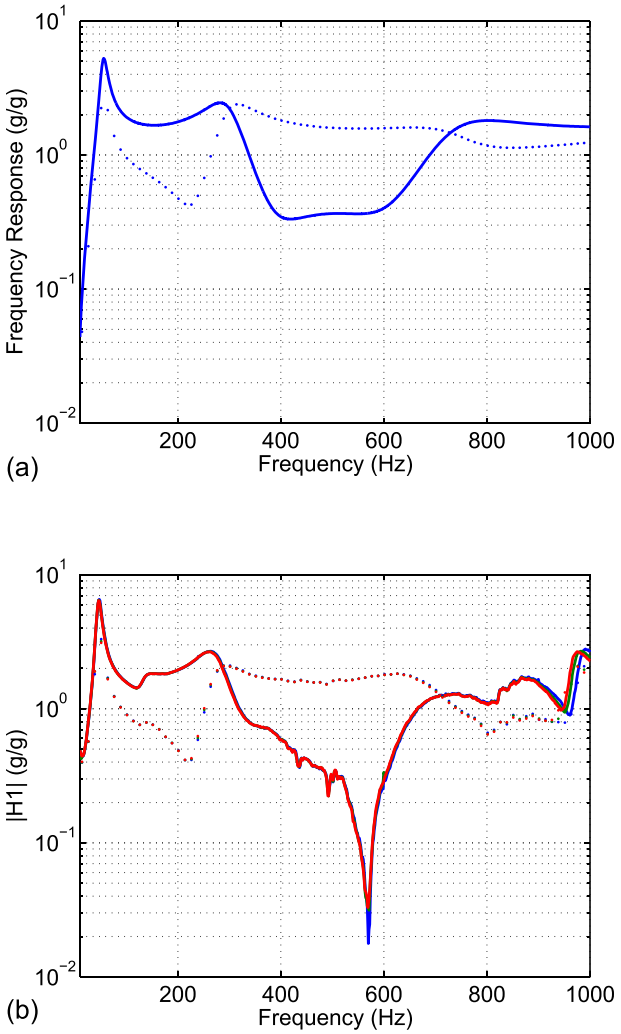

FIG. 2. (a) Analytically modeled frequency response of a 50% plate compared to (b) the experimental H1 mechanical frequency response estimator for three levels of excitation. The red, blue and green curves depict responses at 2.44, 1.86, and 1 g RMS, respectively. Solid lines represent data from the geometric center, and dashed lines represent data from the offset point. Note the multiple clear resonant frequencies, and small differences between force curves. Data are presented for the first set 50% plate.

[This article is copyrighted as indicated in the article. Reuse of AIP content is subject to the terms at: http://scitation.aip.org/termsconditions. Downloaded to] IP: 128.211.168.1 On: Tue, 30 Dec 2014 20:52:05

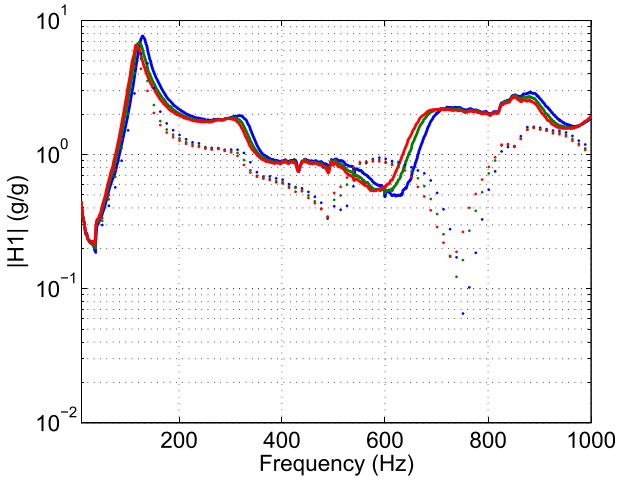

FIG. 3. H1 mechanical frequency response estimators of the first set 65% plate for three levels of excitation. The red, blue and green curves depict responses at 2.44, 1.86, and 1 g RMS, respectively. Solid lines represent data from the geometric center, and dashed lines represent data from the offset point. Note the slightly split first peak, and slightly softening nature of the responses.

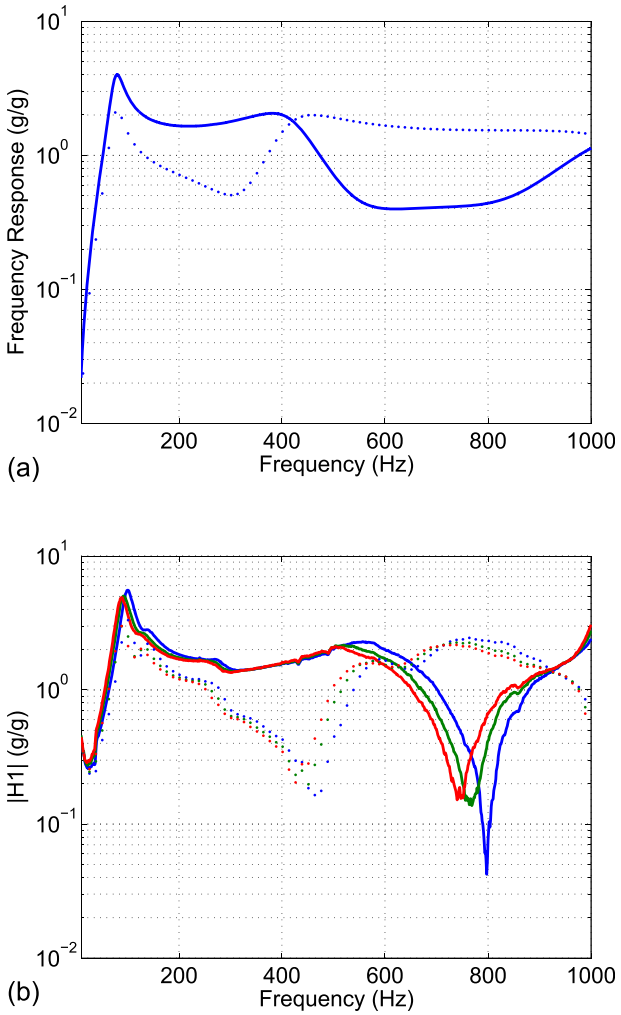

FIG. 4. (a) Analytically modeled frequency response of a 75% plate compared to (b) the experimental H1 mechanical frequency response estimator for three levels of excitation. The red, blue and green curves depict responses at 2.44, 1.86, and 1 g RMS, respectively. Solid lines represent data from the geometric center, and dashed lines represent data from the offset point. Note the split first peak, slightly softening nature of the responses, and comparatively high damping. Data are presented for the first set 75% plate.

TABLE II. Peak mechanical response frequencies for all of the observed operational deflection shapes.

Plate	f_{11} (Hz)	f_{11B} (Hz)	f_{13} (Hz)	f_{13}/f_{11}	f_{31} (Hz)	f_{31}/f_{11}
Analytical (50%)	56.3	—	—	—	282.2	5.01
50%-1	46.3	—	148.8	3.22	261.3	5.65
50%-2	43.8	—	136.3	3.11	243.8	5.57
65%-1	118.8	—	295.0	2.48	—	—
65%-2	98.8	—	296.3	3.00	—	—
Analytical (75%)	80.1	—	—	—	381.1	4.76
75%-1	88.8	113.8	241.3	2.72	505.0	5.69
75%-2	73.8	—	—	—	470.0	6.37
75%-3	72.5	—	—	—	512.5	7.07

clamped and free directions, respectively. Any mode designated with a "1" as the second descriptor is a beam mode, in which no significant deflection is seen in the free direction. The frequencies are grouped by perceived matches between the deformation patterns within each operational deflection shape, and each frequency is nondimensionalized by the first peak value to allow for comparison between cases. As evident from the table, there is generally very good agreement between the nondimensionalized peak frequencies of the observed modes. Table III presents the estimated quality factors of the 11 and 31 modes for each plate. The data points presented are the only ones for which the half-power method was applicable, with the other half-power levels obscured due to relatively low peak magnitudes or overlapping effects from adjacent peaks. It is clear from the H1 estimators and tabulated quality factors that the plates exhibit very distinct modal responses, suggesting that the material is susceptible to excitation through external means.

B. Thermal response

The average of three transient surface temperature responses of each plate at the first resonance, presented separately as the spatial average and maximum surface temperatures of the plate, are presented in Figure 5. As visible in the figure, all of the plates asymptotically approach steady-state within a 60 min window. The mean temperatures of the 50% plates exceed the responses of the 65 and 75% plates. Between the two sets of plates with higher particle/binder ratio, little conclusion may be drawn. The maximum temperature plot reveals that, although the 50% plates still exhibited

TABLE III. Experimentally recovered quality factors.

Plate	Q_{11}	Q_{31}
50%-1	3.70	2.61
50%-2	3.89	1.70
65%-1	4.52	—
65%-2	3.76	—
75%-1	3.38	2.09
75%-2	1.97	—
75%-3	3.22	—

[This article is copyrighted as indicated in the article. Reuse of AIP content is subject to the terms at: http://scitation.aip.org/termsconditions. Downloaded to] IP: 128.211.168.1 On: Tue, 30 Dec 2014 20:52:05

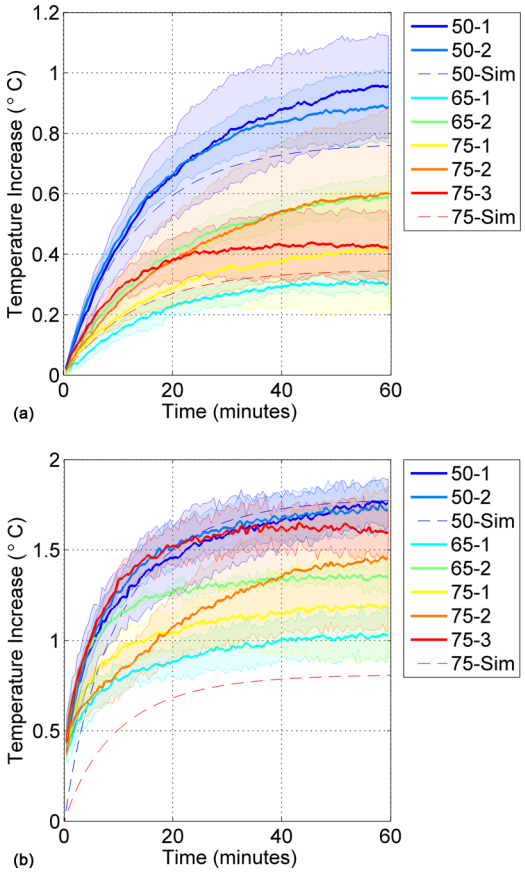

FIG. 5. Comparison of the experimentally obtained plate surface temperatures vs. time in response to a 2 g excitation near the first resonant frequency for all plates. Solid lines indicate experimental data, each the average of three distinct trials per plate. The colored envelope indicates one standard deviation for each trial. Dotted lines indicate numerical simulation data. Data are presented for (a) mean and (b) maximum plate surface temperatures vs. time.

the greatest thermal response, certain 75% plates were quite comparable. Comparisons of the spatial surface temperature profiles and the spatial displacement profiles at the first resonance are presented for each plate type in Figures 6–9. For the 50% and 65% cases, there is good agreement in both the absolute levels of heating and the spatial distributions. For conciseness, a single set of data is presented for each of these ratios. The 75% plates exhibit a greater diversity of behavior. The second and third set 75% plates exhibit significantly different heating patterns from the first due to the degenerate first operational deflection shape exhibited by the first set sample.

The extraneous hot spot exhibited by the first sample 75% plate in Figure 8 was identified as the location of a crack in the plate's surface. As previously outlined, stress concentrations, such as this defect, are often the target of heating in vibrothermography applications. As the temperature level recorded in the defect is at the same level as the patterns developed due to the resonant vibration, the effect of this defect on the maximum temperature data, as presented in Figure 5(b), is considered to be minimal. The effect on the mean temperature response, as presented in Figure 5(a), is more substantial, but quantitatively unknown.

Interestingly, the thermal analysis of higher-frequency operational deflection shapes exhibited some evidence of parity with expected experimental stress levels, but the extremely low levels of heating recorded do not allow for acceptable inclusion at this time.

An additional 75% plate was damaged through the application of a low-frequency (20 Hz) direct excitation at 6 g for less than one minute. A significant change in all of the mechanical-domain responses was noted, with peak frequencies decreasing significantly. The plate did not exhibit any signs of external damage, such as surface cracks or stiffness discontinuities. Therefore, it is expected that the plate was damaged internally, possibly due to a growth in voids or some particle-scale effect. The maximum temperature increase in this plate was significantly greater than all other plates, up to a maximum of 1.4 °C. Due to the unknown nature of this damage, the data are not presented in full form here.

IV. DISCUSSION

A. Viscoelastic heating model

As a point of comparison to the experimental mechanical responses, an analytical solution to the experimentally realized, clamped-free-clamped-free (CFCF) plate vibration problem was approximated through the superposition of clamped-clamped and free-free beam functions as in Warburton.[21] While interaction between the clamped and free components of vibration may be realistically expected for higher modes, at low frequencies this superposition model generates very similar operational deflection shapes to their experimentally observed counterparts. As in the reported experiment, the first few modes were investigated, and the beam superposition model provides a valid point of comparison. The frequency response and operational deflection shapes of each plate were then calculated through modal projection with inertial forcing provided by a prescribed acceleration. The material was assumed to be viscoelastic and to have a complex dynamic modulus. The real part of this modulus for the 50% and 75% plates were estimated as 46.5 and 83.6 MPa, respectively, from uniaxial compression tests.[20] The densities were taken as the average of the data presented in Table I, or 1152 and 1078 kg/m^3 for the 50% and 75% plates, respectively. The structural loss factors were estimated as the inverse of the average experimental quality factors of the first resonant peak of the 50% and 75% plates as 0.26 and 0.35, respectively. The Poisson's ratio was estimated as 0.39, based on perceived material similarities to more common materials such as neoprene rubber.

The peak frequency response values corresponding to various analytical modes are presented in Table II. As evident in the table, the nondimensionalized frequency response peaks of the analytical models seem to provide a decent analog to the experimental data. In addition, the frequency responses of the analytical models are presented in Figures 2 and 4. As evident in the figures, the viscoelastic model appears to provide a good qualitative match for the experimental data, accurately reproducing most of the behaviors

[This article is copyrighted as indicated in the article. Reuse of AIP content is subject to the terms at: http://scitation.aip.org/termsconditions. Downloaded to] IP: 128.211.168.1 On: Tue, 30 Dec 2014 20:52:05

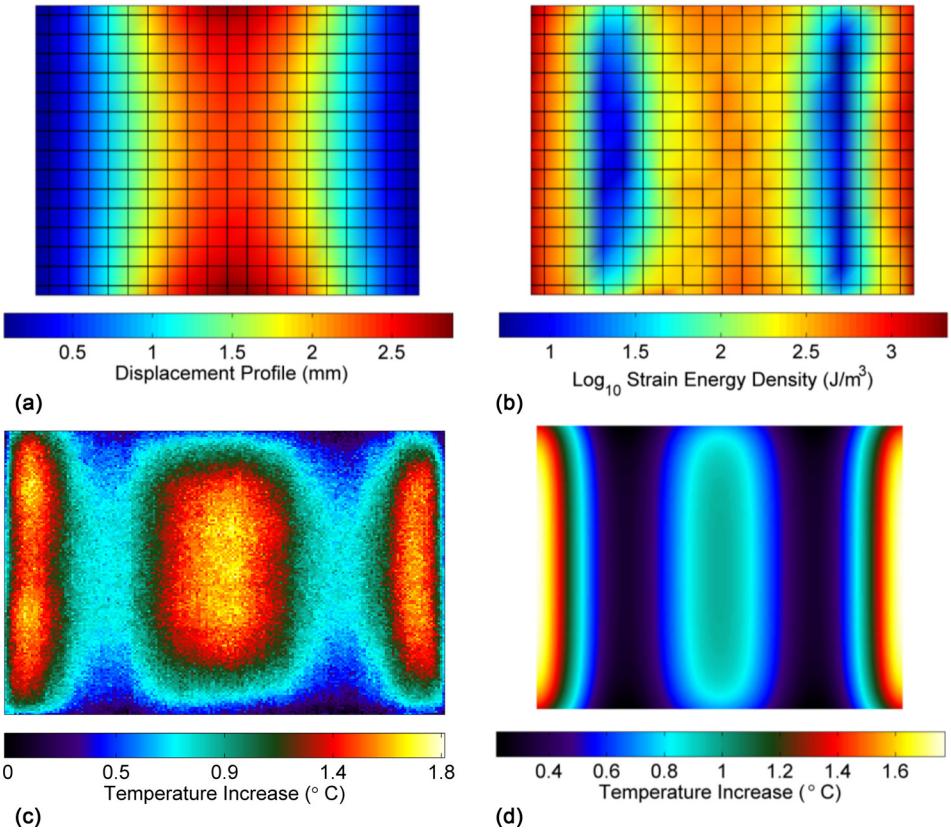

FIG. 6. Comparison of the (a) observed displacement profiles, (b) isotropically predicted strain energy density patterns, and (c) steady-state surface temperature distribution of the second set 50% plate at first resonance to (d) the steady-state surface temperature of a numerically simulated 50% plate.

seen in the frequency response data. This model suggests that a viscoelastic damping term can suitably capture dissipative effects, and that the experimental plates exhibit behavior consistent with classical plate mechanics.

A viscoelastic heat generation model was also considered. Considering a homogeneous model for heat diffusion in three dimensions through the Fourier Law of Conduction, the heat transfer equation is[22]

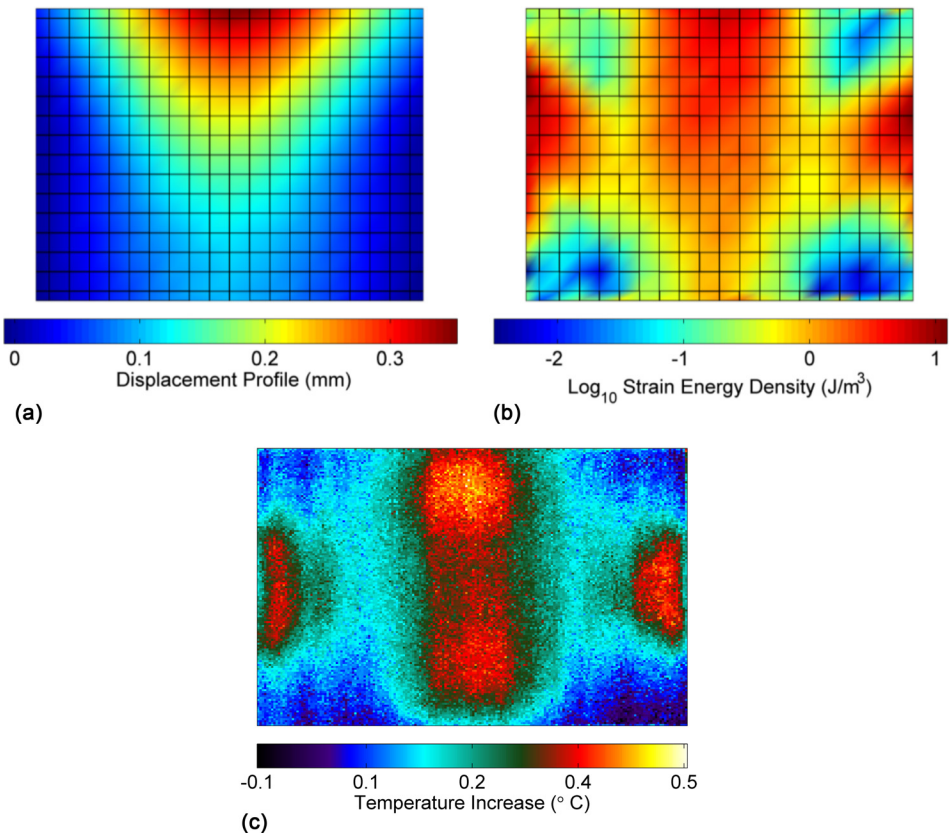

FIG. 7. Comparison of the (a) observed displacement profile, (b) isotropically predicted strain energy density pattern, and (c) steady-state surface temperature distribution of the first set 65% plate at the first resonance.

[This article is copyrighted as indicated in the article. Reuse of AIP content is subject to the terms at: http://scitation.aip.org/termsconditions. Downloaded to] IP: 128.211.168.1 On: Tue, 30 Dec 2014 20:52:05

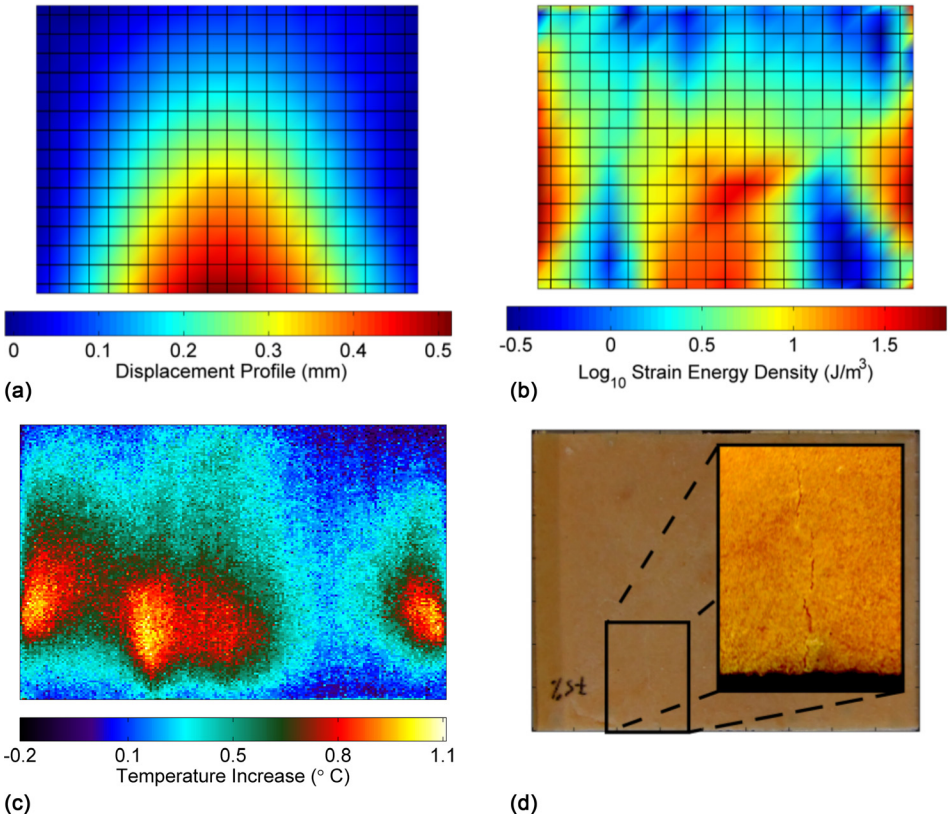

FIG. 8. Comparison of the (a) observed displacement profiles, (b) isotropically predicted strain energy density patterns, and (c) steady-state surface temperature distributions of the defective first set 75% plate at the first resonance. The extraneous heating visible in (c) was noted to coincide with the location of a surface crack, presented (d) as a color-altered photo.

$$\frac{\partial^2\theta}{\partial x^2}+\frac{\partial^2\theta}{\partial y^2}+\frac{\partial^2\theta}{\partial z^2}+\frac{1}{k}r=\frac{1}{\alpha}\frac{\partial\theta}{\partial t}, \tag{1}$$

where θ is the temperature relative to ambient, x, y, and z are the spatial locations along the beam axis, the transverse axis, and the surface normal, respectively, k is the thermal conductivity, α is the thermal diffusivity, and r is the volumetric energy generation.

Over one cycle of harmonic loading, the mechanical energy dissipated in the plate can be estimated as the area

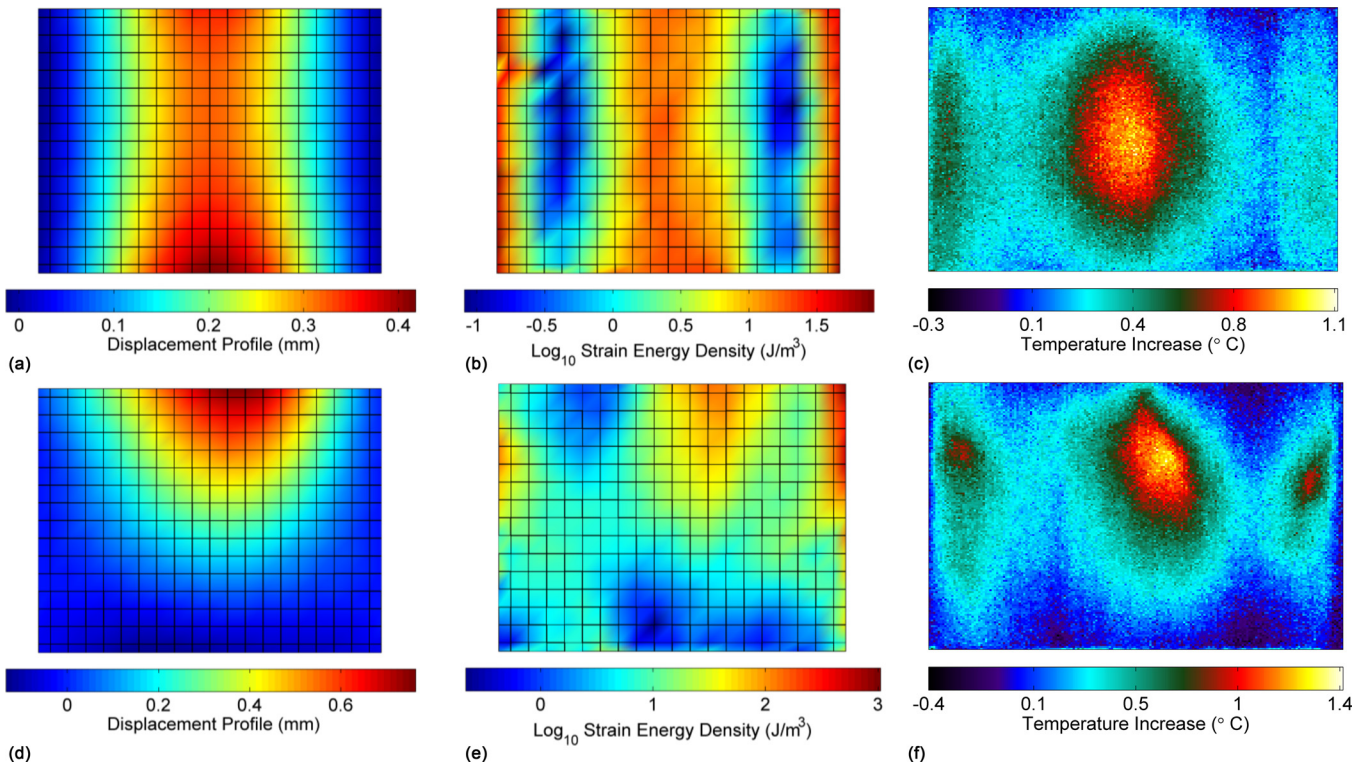

FIG. 9. Comparison of [(a) and (d)] the observed displacement profiles, [(b) and (e)] isotropically predicted strain energy density patterns and [(c) and (f)] steady-state surface temperature distributions of the second and third set 75% plates at the first resonance.

[This article is copyrighted as indicated in the article. Reuse of AIP content is subject to the terms at: http://scitation.aip.org/termsconditions. Downloaded to] IP: 128.211.168.1 On: Tue, 30 Dec 2014 20:52:05

under the hysteresis loop of the stress-strain plot in the mechanical steady-state.[23] Making the assumption that the temperature variation occurs on a much slower time scale than the mechanical loading, the volumetric energy generation may be time-averaged over one mechanical loading cycle.[24] Assuming the energy is solely dissipated as heat, the time-averaged volumetric energy generation is given by[19]

$$r_{avg} = \frac{\omega}{2\pi}\int_{t_0}^{t_0+\frac{2\pi}{\omega}} \sigma \frac{\partial \epsilon}{\partial \tau} d\tau = \pi_0(\eta\omega), \tag{2}$$

where η is the loss factor, ω is the frequency of excitation, and π_0 is the strain energy density given by

$$\pi_o = \frac{E'\epsilon_0^2}{2(1-\nu^2)}, \tag{3}$$

where E' is the real part of the dynamic modulus of the plate, ν is Poisson's ratio, and ϵ_0 is the strain magnitude.

B. Strain estimation

As evident from Eq. (2), the heat source anticipated by viscoelastic theory is directly dependent on the strain energy density. To investigate this correlation, the strain energy densities within the plates were estimated through the application of isotropic theory. For this calculation, the plates were assumed to be thin compared to the length and the transverse shear and normal strain components were assumed to be negligible. As in Rao,[25] the strain components may be calculated as derivatives of the out-of plane displacement, in this case computed as fifth-order centered numerical derivatives. The following calculations were completed numerically on a grid of integrated velocity measurements recorded via laser Doppler vibrometry:

$$\begin{aligned}\epsilon_{xx} &= -z\frac{\partial^2 w}{\partial x^2},\\ \epsilon_{yy} &= -z\frac{\partial^2 w}{\partial y^2},\\ \epsilon_{xy} &= -2z\frac{\partial^2 w}{\partial x \partial y},\end{aligned} \tag{4}$$

where w represents the experimental, vibrometry-measured surface displacement. Assuming an isotropic material and utilizing material properties as in the analytical model (while reusing the estimated Young's Modulus for the 50% plate in lieu of a measured 65% value), the state of stress may be easily computed

$$\begin{aligned}\sigma_{xx} &= \frac{E}{1-\nu^2}(\epsilon_{xx}+\nu\epsilon_{yy}),\\ \sigma_{yy} &= \frac{E}{1-\nu^2}(\epsilon_{yy}+\nu\epsilon_{xx}),\\ \sigma_{xy} &= \frac{E}{2(1+\nu)}\epsilon_{xy}.\end{aligned} \tag{5}$$

Finally, the strain energy density may be calculated as

$$\pi_0 = \frac{1}{2}(\sigma_{xx}\epsilon_{xx} + \sigma_{yy}\epsilon_{yy} + \sigma_{xy}\epsilon_{xy}) \tag{6}$$

The results of these strain energy density calculations are presented in log form within Figures 6–9. As evident in the figures, there is a strong correlation between areas of estimated strain energy density and temperature response, as predicted by Eq. (2).

C. Thermal simulation

As a point of comparison to the experimental temperature responses, the response of a representative plate to the heat source derived in Eq. (2) was simulated with a commercial finite element package. For a Kirchhoff plate, where mid-plane deflection is small, the value of ϵ_0 depends on the transverse position, z, and spatial derivatives of the modal displacement obtained from the beam superposition model, $\tilde{u}(x,y)$.

$$\epsilon_0^2(x,y,z) = z^2\left[\left(\frac{\partial^2\tilde{u}}{\partial x^2}\right)^2 + \left(\frac{\partial^2\tilde{u}}{\partial y^2}\right)^2 + 2\nu\left(\frac{\partial^2\tilde{u}}{\partial x}\frac{\partial^2\tilde{u}}{\partial y}\right) + 2(1-\nu)\left(\frac{\partial^2\tilde{u}}{\partial x\partial y}\right)^2\right]. \tag{7}$$

For a thin plate, the volumetric energy generation can be spatially averaged over the thickness.[26] This gives the two-dimensional heat source

$$r(x,y) = \frac{E\eta\omega h^2}{24(1-\nu^2)}\left[\left(\frac{\partial^2\tilde{u}}{\partial x^2}\right)^2 + \left(\frac{\partial^2\tilde{u}}{\mathrm{d}y^2}\right)^2 + 2\nu\left(\frac{\partial^2\tilde{u}}{\partial x}\frac{\partial^2\tilde{u}}{\partial y}\right) + 2(1-\nu)\left(\frac{\partial^2\tilde{u}}{\mathrm{d}x\partial y}\right)^2\right]. \tag{8}$$

The transient thermal behavior of a representative plate with this heat source was simulated, assuming insulated clamped ends and convective boundaries elsewhere. The thermal properties of a representative 75% plate were measured using the transient plane source technique.[27] Due to the small absolute level of temperature fluctuations considered, the effects of thermal expansion are neglected. The thermal conductivity (k) and thermal diffusivity (α) were measured as 0.52 W/(m-K) and 3.13×10^{-7} m^2/s, respectively. The convection coefficient (h) was estimated as 13 W/(m^2-K) in an attempt to match the transient maximum temperature behavior observed experimentally in the 50% plates and is assumed to not change dramatically between plates. This value is comparable with coefficients found in experimental investigations[28–30] and is within the range for free convection estimates presented in Incropera *et al.*[22]

The finite element simulation was used to generate simulations of transient behavior over 60 min as well as top-down thermal profiles, which allow for direct comparison to the experimentally obtained thermal images. As evident in Figure 5, with the current selection of convective coefficient the numerical simulation very closely matches the transient data for the 50% plates in a qualitative way. The 75% plates,

[This article is copyrighted as indicated in the article. Reuse of AIP content is subject to the terms at: http://scitation.aip.org/termsconditions. Downloaded to] IP: 128.211.168.1 On: Tue, 30 Dec 2014 20:52:05

however, exhibited thermal responses at a much higher magnitude than predicted through this simple, viscoelastic model. This would suggest that an additional mechanism elicits a thermal response from these high particle/binder ratio plates.

The steady-state temperature profile predicted for the 50% case is presented in Figure 6. The prediction echoes the experimental data with three bands of temperature concentration but appears to be more highly concentrated at the clamped edges. This discrepancy may be due to the imperfect experimental clamps, which allow for some rotation, and the insulated boundary assumptions, which would not accurately account for conduction into the experimental clamping fixture. The 75% thermal profile is not presented due to its qualitative similarities to the 50% result, which is different only in scale as obvious in the transient temperature data presented in Figure 5.

V. CONCLUSIONS

The thermal and mechanical responses of particulate composite plates, composed of various ratios of NH_4Cl particles and HTPB binder, under direct excitation have been presented. Each plate was shown to exhibit clear resonant behavior with several distinct operational deflection shapes. The results presented herein reveal near-resonant behaviors that are strongly dependent on the particle/binder volume fraction associated with the sample. For example, an increase in the volume of particles relative to binder appears to increase the effective bulk damping level within the material. This effect is likely due to internal friction effects attributable to particle-particle interactions at the micro-scale.

The reported steady-state surface temperature profiles appear to exhibit patterns in agreement with isotropically predicted strain energy density fields. In general, the thermal response echoes the state of stress in the material. This conclusion is supported by the defective first set 75% plate, which shows high levels of thermal response around a surface crack. As illustrated by the high-magnitude thermal response of the 50% plates, heating appears to be maximized for highly viscous materials. As classically predicted, thermal effects will be maximized when the phase delay between stress and strain is maximized—an effect congruent with highly viscous materials. The level of heating, however, also appears to rise with high crystal volume ratios as with the response of the second and third set 75% plates, high above the amount predicted by a simple viscoelastic model. This effect is likely due to interactions on the particle scale, where direct particle interactions may lead to significant stress concentrations exacerbated by the resonant excitation. A similar effect has been observed at ultrasonic frequencies.[31] This effect may be exploited to elucidate significant thermal responses within high particle/binder ratio particulate composite structures. Additionally, in the case of the low-frequency damaged 75% plate, heating was seen to increase dramatically after short-duration high-amplitude excitation due to an unknown internal effect.

The observed heating effects could be used in support of current trace vapor detection methods to increase the vapor concentrations of explosives. While the absolute levels of temperature increase are as of yet below what may be effective in this regard, it is hoped that through targeted excitation the effect may be exacerbated. It is expected that the same heating phenomena observed via the direct excitation utilized in this work could be excited by stand-off acoustic sources. As low-frequency excitation may be used over long distances, such excitation could prove effective at stand-off heating, thus enabling the detection of relatively large, hidden explosive devices in a fieldable detection system.

The selective targeting of higher-frequency resonant peaks did not reveal significant heat generation. The complexity of the operational deflection shapes predicts a significant increase in the forcing required to achieve the same levels of strain and, theoretically, similar thermal responses. It is thus expected that higher-frequency resonant peaks will not be as efficient for thermal energy delivery, and that hypothetical stand-off excitation systems would be best suited to target a structure's first resonance.

Future work will attempt to more completely investigate the relationship between particle/binder ratio and the thermomechanical responses of various particulate composite materials, including plastic-bonded explosives, through theory and experimentation. The use of stand-off excitation will also be addressed, assessing the viability of targeting the observed heating effects in more realistic scenarios.

ACKNOWLEDGMENTS

This research is supported by the U.S. Office of Naval Research under the Multidisciplinary University Research Initiative on "Sound and Electromagnetic Interacting Waves" through Grant No. N00014-10-1-0958. The authors wish to acknowledge Chris Watson and Professor Douglas Adams for their efforts related to sample preparation, Jelena Paripovic and Professor Patricia Davies for mechanical property measurements, and Jesus Mares and Professor Steve Son for thermal property measurements. A preliminary version of this work was presented in the proceedings of the ASME IDETC/CIE 2013 conference.[32]

[1]D. S. Moore, Sens. Imaging: Int. J. **8**, 9 (2007).
[2]D. S. Moore, Rev. Sci. Instrum. **75**, 2499 (2004).
[3]A. V. Kuznetsov and O. I. Osetrov, in *Detection and Disposal of Improvised Explosives*, NATO Security through Science Series, edited by H. Schubert and A. Kuznetsov (Springer, Netherlands, 2006) pp. 7–25.
[4]S. B. Ratner and V. I. Korobov, Polym. Mech. **1**, 63 (1965).
[5]J. Renshaw, J. C. Chen, S. D. Holland, and R. B. Thompson, NDT & E Int. **44**, 736 (2011).
[6]O. P. Chervinko, Int. Appl. Mech. **40**, 916 (2004).
[7]O. P. Chervinko, I. K. Senchenkov, and N. N. Yakimenko, Int. Appl. Mech. **43**, 647 (2007).
[8]W. Luo, T. Yang, Z. Li, and L. Yuan, Int. J. Solids Struct. **37**, 887 (2000).
[9]R. B. Mignogna, R. E. Green, Jr., J. C. Duke, Jr., E. G. Henneke II, and K. L. Reifsnider, Ultrasonics **19**, 159 (1981).
[10]W. Zhang, "Frequency and load mode dependence of vibrothermography," Master's thesis (Iowa State University, 2010).
[11]A. Katunin and M. Fidali, Polym. Compos. **33**, 138 (2012).
[12]E. G. Henneke II, K. L. Reifsnider, and W. W. Stinchcomb, "Vibrothermography: Investigation, development, and application of a new nondestructive evaluation technique," Tech. Rep. (DTIC Document AD-A175 373, 1986).
[13]N. P. Loginov, S. M. Muratov, and N. K. Nazarov, Combust., Explosion, Shock Waves **12**, 367 (1976).

[This article is copyrighted as indicated in the article. Reuse of AIP content is subject to the terms at: http://scitation.aip.org/termsconditions. Downloaded to] IP: 128.211.168.1 On: Tue, 30 Dec 2014 20:52:05

[14]N. P. Loginov, Combust., Explosion, Shock Waves **33**, 598 (1997).
[15]K. Wakashima and H. Tsukamoto, Mater. Sci. Eng.: A **146**, 291 (1991).
[16]S.-Y. Fu, X.-Q. Feng, B. Lauke, and Y.-W. Mai, Compos. Part B: Eng. **39**, 933 (2008).
[17]R. Arefinia and A. Shojaei, J. Colloid Interface Sci. **299**, 962 (2006).
[18]T. B. Lewis and L. E. Nielsen, J. Appl. Polym. Sci. **14**, 1449 (1970).
[19]D. C. Woods, J. K. Miller, and J. F. Rhoads, "On the Thermomechanical Response of HTPB-Based Composite Beams Under Near-Resonant Excitation," J. Vib. Acoust. (submitted).
[20]J. Paripovic, Personal Communication (2013).
[21]G. B. Warburton, Proc. Inst. Mech. Eng. **168**, 371 (1954).
[22]F. P. Incropera, D. P. DeWitt, T. L. Bergman, and A. S. Lavine, *Introduction to Heat Transfer* (John Wiley & Sons., 2007).
[23]H. F. Brinson and L. C. Brinson, *Polymer Engineering Science and Viscoelasticity: An Introduction* (Springer, 2008).
[24]F. Dinzart, A. Molinari, and R. Herbach, Arch. Mech. **60**, 59 (2008), can be found at http://am.ippt.gov.pl/index.php/am/article/view/v60p59.
[25]S. S. Rao, *Vibration of Continuous Systems* (John Wiley & Sons, Inc, 2007).
[26]A. D. Dimarogonas and N. B. Syrimbeis, J. Sound Vib. **157**, 467 (1992).
[27]S. E. Gustafsson, Rev. Sci. Instrum. **62**, 797 (1991).
[28]B. R. Rich, Trans. ASME **75**, 489 (1953).
[29]G. C. Vliet, J. Heat Transfer **91**, 511 (1969).
[30]R. J. Goldstein, E. M. Sparrow, and D. C. Jones, Int. J. Heat Mass Transfer **16**, 1025 (1973).
[31]J. O. Mares, J. K. Miller, N. D. Sharp, D. S. Moore, D. E. Adams, L. J. Groven, J. F. Rhoads, and S. F. Son, J. Appl. Phys. **113**, 084904 (2013).
[32]J. K. Miller and J. F. Rhoads, in *Proceedings of the ASME 2013 International Design Engineering Technical Conferences*, DETC2013-12138 (2013).

[This article is copyrighted as indicated in the article. Reuse of AIP content is subject to the terms at: http://scitation.aip.org/termsconditions. Downloaded to] IP: 128.211.168.1 On: Tue, 30 Dec 2014 20:52:05